Reviews of Electromagnetics
EuCAP 2025 Special Issue

Suppression of the Polarization-Dependent Antenna Carrier Effect in Phased Arrays with Electromagnetic Bandgaps for Airborne SAR Applications

Diego Lorente[1]*, Markus Limbach[1], Bernd Gabler[1], Héctor Esteban[2], Vicente E. Boria Esbert[2]

Abstract

The polarization-dependent edge diffraction effects due to the interaction between the antenna and the carrier structure, that enables the antenna mounting on the aircraft, is presented in this paper. The resulting antenna carrier impact is experimentally verified, by means of measurements performed with the operational flight-certified L-band phased array antenna employed in the next-generation DLR bistatic airborne Synthetic Aperture Radar (SAR) sensor. Measured radiation pattern in elevation shows a main beam widening and gain reduction of approximately 1 dB for the vertical polarization, that becomes more sensitive to edge diffraction effects due to the electric field direction and the carrier geometry. On the other side, the performance of the horizontal polarization remains unaffected. In order to achieve a similar radiation response for both polarizations that is required in polarimetric SAR systems, the use of Electromagnetic Bandgaps (EBGs) is proposed. Making use of the surface wave suppression properties of EBGs, the induced currents on the carrier for the vertical polarization can be mitigated, thus reducing the resulting edge diffraction effects without affecting the performance of the horizontal polarization. The presented approach is validated with measurements placing EBGs on each side of the antenna carrier surface. This way, a comparable radiation features for both polarizations can be achieved, that become independent of the carrier structure.

Key terms

airborne SAR, dual-linear polarization, phased array, antenna carrier, antenna interaction, surface wave, edge diffraction effects, Electromagnetic Bandgaps

1. Introduction

The rising interest in Earth surface monitoring systems, boosted by the growing concern on global warming and climate change, has established Synthetic Aperture Radar (SAR) as one of the most important remote-sensing techniques of our time.

SAR provides high-resolution, distance-independent imaging data with all-weather, and day-and-night operational capabilities [1]. Exploiting the electrical properties of electromagnetic waves, SAR covers a wide range of application areas. By means of interferometry, that makes use of the phase information,

SAR sensors can generate digital elevation models to analyze the terrain topography [2]. Taking advantage of the penetrating capabilities of electromagnetic waves at lower frequencies, SAR allows to perform forest density analysis and forest height estimation by means of tomography, as well as subsurface imaging [3]. Another important technique is SAR polarimetry, that exploits the polarization diversity to identify different scattering mechanisms, and thus enhance the retrieval of information [4].

Airborne SAR sensors are employed in order to support the technological development of future spaceborne SAR missions.

For this reason, they become an intense research subject due to its operational flexibility [5]-[7].

On the one side, the design of airborne SAR antennas is driven by the electrical requirements determined by the system operation, such as beam steering, frequency, bandwidth or dual-linear polarization to apply polarimetry. On the other side, different demanding mechanical specifications have to be met in order to fulfill the airworthiness requirements of airborne applications. For this reason, the airborne antenna has to be mounted on an specific aerodynamic structure, known as antenna carrier, that enables its installment on the aircraft.

Inevitably, the electromagnetic fields radiated by the antenna interact with its environment. Since airborne antennas are usually surrounded by metallic structures, such as the aircraft fuselage or the antenna carrier, and due to the propagation of the radiated fields that can extend many wavelengths, surface waves are induced onto these structures. The wave interaction with the antenna environment can lead to unwanted scattering effects, such as edge diffraction coming from discontinuities of the surrounding geometry, as well as to multipath interference (due to the contribution of different propagating waves) causing signal distortion.

Thus, the interaction of the antenna with its environment can affect its radiation performance, causing gain reduction or amplitude ripple, radiation enhancement at undesired directions, such as side lobes or back lobes, as well as the increase of the cross-polarization levels. Some well-known approaches make use of choke rings [8, 9], or metamaterial-based absorbers [10] to mitigate the multipath effect in navigation applications or as an antenna shielding [11]. However, choke rings can become bulky solutions, especially at lower frequencies, and the use of microwave absorbers can lead to pattern distortion or loss of desired radiated energy, particularly if they are placed too close to the antenna. Other approaches take advantage of the stop-band properties of Electromagnetic Bandgaps (EBGs), to synthesize a high impedance surface, thus enhancing the radiation properties of the antenna [12, 13], or to reduce the interference between array elements [14, 15]. Due to its miniaturization and integration capabilities, as well as its low-profile characteristics, EBGs become a suitable solution in order to mitigate the antenna external interactions in airborne applications, thus achieving a more independent radiation performance regardless of the antenna environment.

Edge diffraction effects are usually analyzed considering single antennas mounted on finite ground planes [16, 17], as well as in planar arrays applications [18]-[20], including also the scanning performance of single-polarized phased array antennas [21]. In [22], a dual-polarized phased array for weather radar applications is considered for the analysis of edge diffraction effects. To the best of author's knowledge, only in [23] the polarization-dependent beam-steering impact of the edge diffraction effects in dual-linear polarized airborne SAR antennas, and how to suppress them using EBGs, has been presented. In this work, the latter proposed approach is experimentally validated by means of measurements considering a real airborne SAR scenario that includes the flight-certified antenna hardware installed on the carrier platform.

This paper is structured as follows: in section 2, the electrical details of the airborne SAR antenna, and how it is installed on the aircraft by means of the antenna carrier platform, is explained. Later, in section 3, the measured antenna performance with the carrier is presented and compared with the stand-alone configuration, including the discussion of the resulting polarization-dependent edge diffraction effects. Next, in section 4, a solution to mitigate the antenna interaction with the carrier using EBGs is proposed, that will be experimentally validated with measurements in section 5. Finally, in the conclusions, the main outcomes of the presented work are discussed.

2. Antenna installation on the aircraft

The next-generation bistatic L-band airborne SAR sensor of the German Aerospace Center (DLR) is operated by means of an L-band planar phased array antenna of $5{\times}8$ elements, with beam steering in elevation at $\theta \approx 45°$ to achieve the side-looking acquisition of SAR systems [24]. The antenna operates at the center frequency $f_0 =$1.325 GHz with a bandwidth of 200 MHz. The antenna aperture is approximately 53 cm $\times$ 85 cm, that is given by the limited available space on the aircraft, thus leading to a low-profile multilayer phased array design with a high degree of integration. The dual-linear polarization capabilities of the antenna allow to exploit the polarization diversity for transmitting and receiving purposes, thus obtaining more information of the imaged area, leading to a better target classification.

The antenna is mounted on the carrier structure, an aerodynamic platform that allows its installment on the aircraft in order to fulfill the airworthiness requirements. The antenna carrier structure, that is attached under the airplane, and it is only flight-certified exclusively for a single aircraft, is shown in Figure 1. It has a circular form, since the overall platform is mechanically adapted to enable a slight rotation of the antennas, thereby achieving different looking angles for bistatic radar measurements. The antenna is placed at the center of a circular plate, that becomes the most relevant electric part of the carrier, due to its proximity to the antenna.

Despite that the antenna carrier refers to the entire platform under the aircraft, for the sake of clarity, only the circular plate will be known as the antenna carrier. The phased array antenna mounted on the center of the antenna carrier is shown in Figure 2.
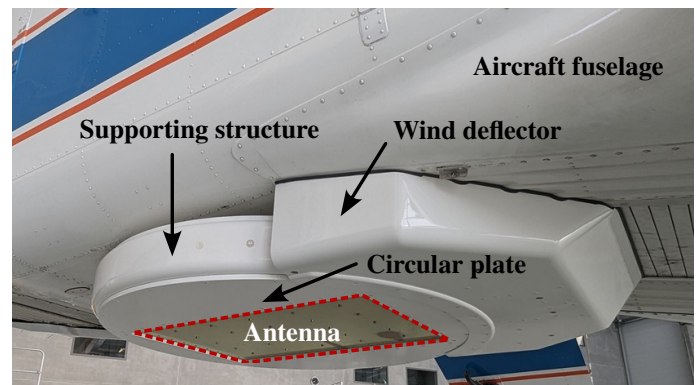

Figure 1: Antenna carrier platform installed under the aircraft.

The antenna carrier has a diameter of 120 cm and thickness 1.27 cm, and it is made of a carbon fiber reinforced (CFR) polymer whose surface is covered with a copper mesh. The metallic surface of the antenna carrier is required to deviate the electrostatic charge that can occur when the aircraft flights through clouds, as well as in the case of a lightning strikes.

The final SAR system operation is strongly determined by the electrical performance of the antenna when mounted on the aircraft. For this reason, the radiation properties of the antenna have to be analyzed considering the resulting interaction of the antenna with the carrier structure.
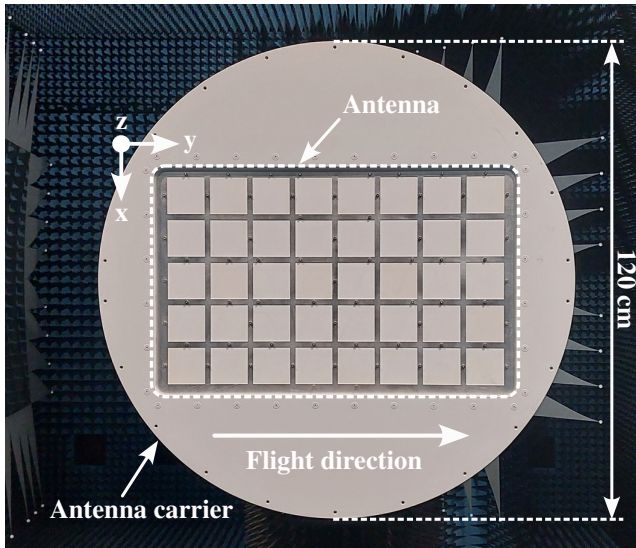

Figure 2: Antenna mounted on the carrier structure during measurements in the DLR's Compact Test Range (CTR).

3. Impact of the edge diffraction effects

The measured radiation pattern in elevation plane (XZ) at the center frequency of operation, for the vertical and horizontal polarization, are shown in Figures 3 and 4, respectively. To properly assess the impact of the antenna carrier, a comparison with the antenna itself (stand-alone configuration) is also provided.

As convention, the vertical polarized fields are aligned along the x-axis, becoming XZ its E-Plane. Thereby, the electric field of the orthogonal polarization is aligned along the y-axis, which corresponds to the flight direction and parallel to the horizon, thus being this polarization the horizontal one.

The measured gain of the antenna in stand-alone configuration (i.e without antenna carrier) is 14.18 dBi and 14.98 dBi for the vertical and horizontal polarization, respectively. When mounted on the antenna carrier, the measured gain drops to 13.27 dBi for the vertical polarization and remains comparable for the horizontal one, with a gain value of 15.1 dBi. It can be noted that, while no noticeable impact of the antenna carrier is visible for the horizontal polarization, for the vertical one a main beam widening occurs along with a gain reduction around 1 dB. This has to be considered twice in the system performance, since due to the two-way operation of SAR sensors, the same antenna is used for transmitting and receiving purposes.
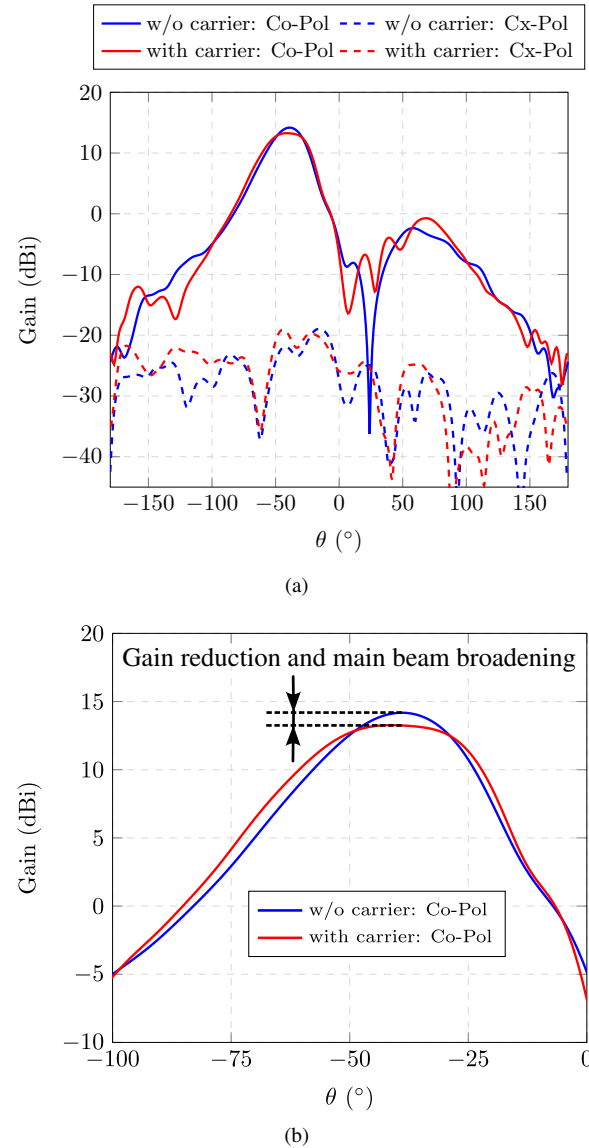

(a)

(b)

Figure 3: Measured radiation pattern at 1.325 GHz. Vertical polarization. Comparison of the stand-alone configuration with the antenna mounted on the carrier. (a) Elevation plane cut. (b) Main beam broadening and gain reduction.

Be noted that, since the antenna carrier is covered with a copper mesh, the surface conductivity could be slightly affected, leading to lower measured gain values. Thus, the gain reduction can be explained as a combination of the not homogeneous carrier surface conductivity along with the edge diffraction effects. In addition, the main beam widening resulting from the edge diffraction effects is also undesired, since this beam broadening affects the illuminated footprint on the ground, leading to different swath widths for each polarization.

Figure 5 plots the measured radiation pattern in azimuth, i.e the YZ plane tilted at the maximum of elevation ($\theta \approx 45°$), and for both polarizations. The carrier effect can also be observed for the vertical polarization. In addition, the cross-polarization levels at this plane are also the highest ones, and are slightly enhanced due to the carrier effect.
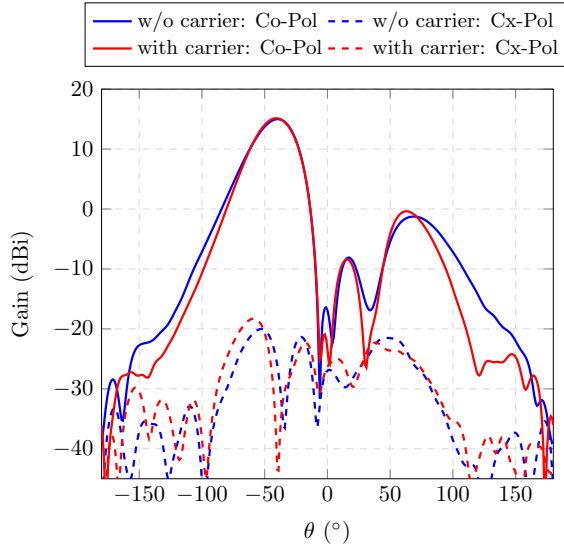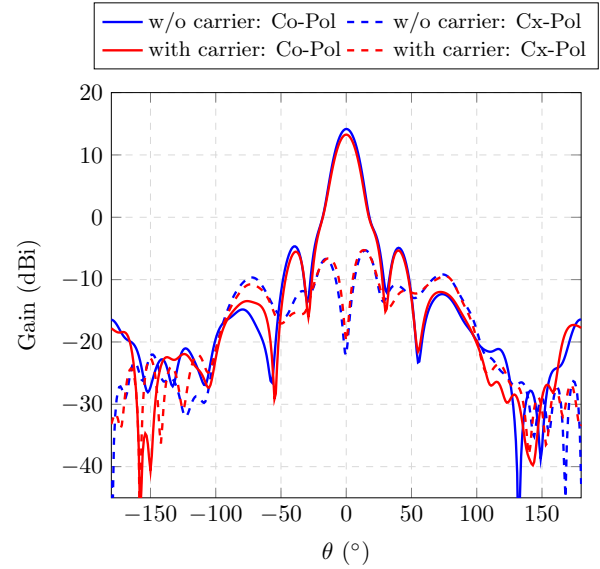
Figure 4: Measured radiation pattern in elevation at 1.325 GHz. Horizontal polarization. Comparison of the stand-alone configuration with the antenna mounted on the carrier.
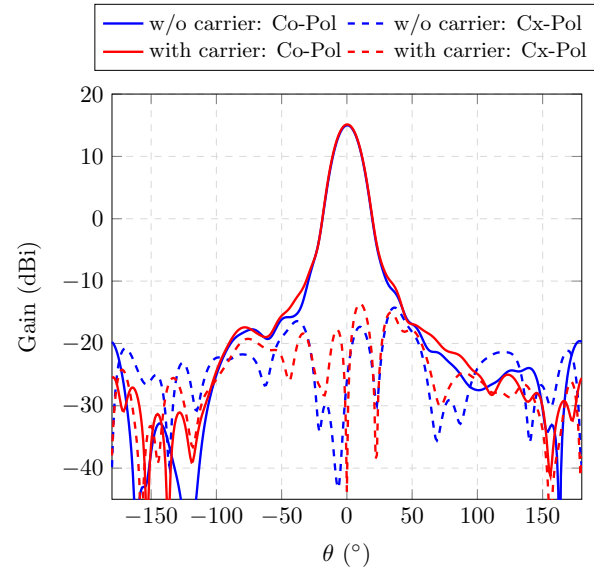
In order to analyze the polarization-dependent interaction of the radiated fields with the carrier, the induced surface currents on the carrier are plotted in Figure 6. The simulation analysis is performed using the full-wave electromagnetic software HFSS. It can be seen that, for the vertical polarization, not only the magnitude of the induced currents is higher but they also propagate along the carrier surface. On the other side, the intensity of the surface currents of the horizontal polarization is lower and they are more concentrated around the antenna aperture.

A similar analysis can be performed when plotting the radiated electric fields in the elevation plane (XZ), depicted in Figure 7. It can be noted that, for the vertical polarization, the radiated fields propagate along the carrier surface unlike the horizontal polarization. This can be explained since the elevation plane, where the beam steering takes place, corresponds to the E-plane of the vertical polarization. Thus, due to the electric field direction and the carrier geometry, the impact of the edge diffraction effects is more visible for the vertical polarization, that is further detailed as follows.

The interaction of the radiated fields with the metallic surface of the carrier generates transversal magnetic (TM) surface waves that propagate along the carrier. These surface waves interact with edges or discontinuities of the surrounding geometry producing diffracted fields. They are combined with the direct radiated field, thus creating constructively and destructively interferences that can distort the radiation pattern, as depicted in Figure 8. The impact of the edge diffraction effects is especially visible in areas with low field intensity, thereby affecting the side lobe level, back lobes, radiation nulls or the cross-polarization performance. In addition, the antenna main beam can be also distorted, especially in the E-Plane, as experimentally validated with the measurement shown in Figure 3. In addition, this beam distortion can get considerably worsened (leading to an amplitude ripple) if the carrier size or the metallic structure is electrically large in E-Plane, as it is shown next.

(a)

(b)

Figure 5: Measured radiation pattern at 1.325 GHz in the azimuth plane. Comparison of the stand-alone configuration with the antenna mounted on the carrier. (a) Vertical polarization. (b) Horizontal polarization.

Figures 9 and 10 plot an analysis of the radiation pattern in elevation considering different carrier sizes for the vertical and horizontal polarization, respectively. It can be seen that the edge diffraction effects become more visible for the vertical polarization when the electrical size of the carrier is increased, leading to an amplitude ripple in the main beam, as well as higher magnitude and further propagation of the surface currents induced on the carrier. On the other side, the impact of the antenna carrier for the horizontal polarization is not electrical relevant, as it is seen by the barely unaffected main beam and the intensity of the induced currents on the carrier surface. Be noted that the analysis for larger carrier sizes (200 cm and 240
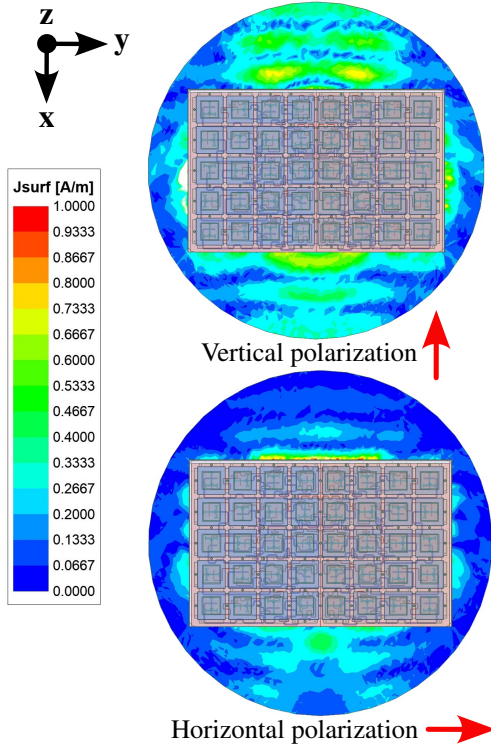
Figure 6: Magnitude of the induced surface currents on the antenna carrier for both polarizations. Each polarization is excited with 100 W input power.
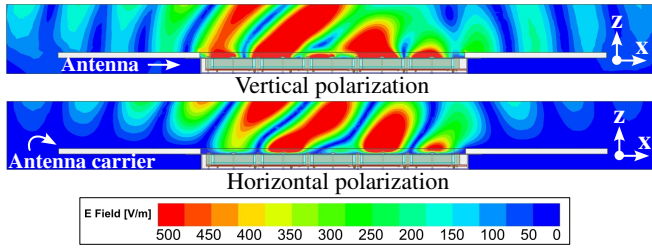

Figure 7: Radiated electric fields for both polarizations in the elevation plane (XZ). Each polarization is excited with 100 W input power.
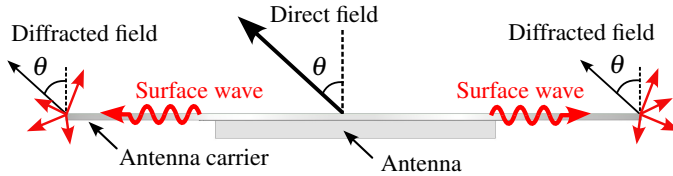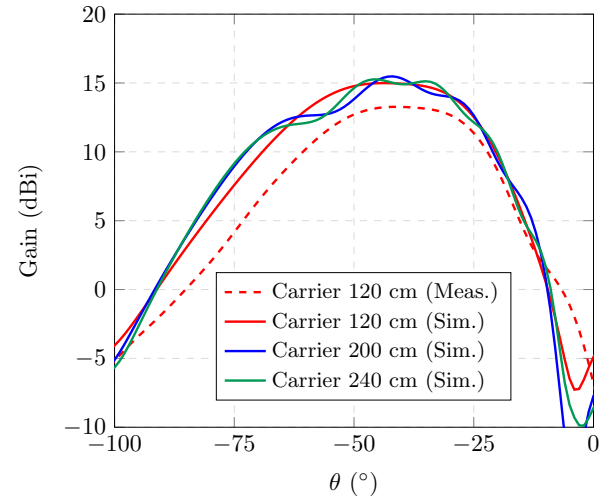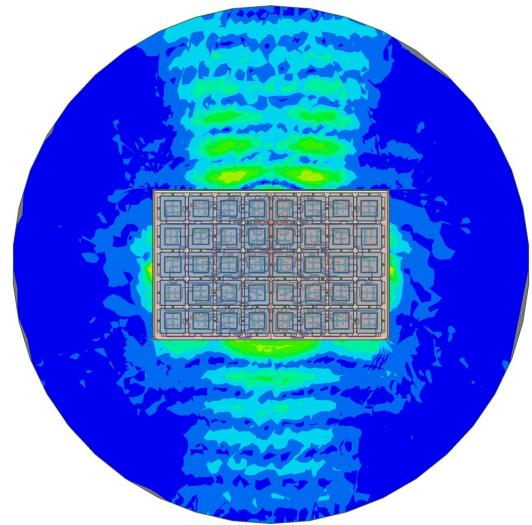

Figure 8: Edge diffraction effects resulting from the interaction of the propagating surface waves with the carrier edges.

cm) is simulated, which leads to higher gain values than the measured results,that become more noticeable for the vertical polarization. This gain difference, that is around 1.5 dB, can be also seen when comparing the results with the antenna mounted on the carrier (120 cm), and it is explained due to the internal feeding network losses, as well as construction and assembly tolerances.

Figure 9: Analysis increasing the electrical size of the carrier. Vertical polarization. (a) Main beam in elevation. (b) Induced surface currents for a carrier diameter of 200 cm.

Be noted that the electrical size of the original carrier, which has a 120 cm diameter, is not electrically large for the operational frequency at L-band but the impact of the carrier is still visible for the vertical polarization. However, for higher frequencies, the size of the antenna surrounding easily becomes many wavelengths in extension, thus being the edge diffraction effects even more noticeable, as the analysis of Figure 10 shows.

Thus, the polarization-dependent edge diffraction effects have to be mitigated, in order to achieve a more comparable radiation performance for both polarizations, that will strongly determine the final SAR system operation. In order to do so, the induced surface currents on the carrier have to be reduced, thus leading to the suppression of surface waves.
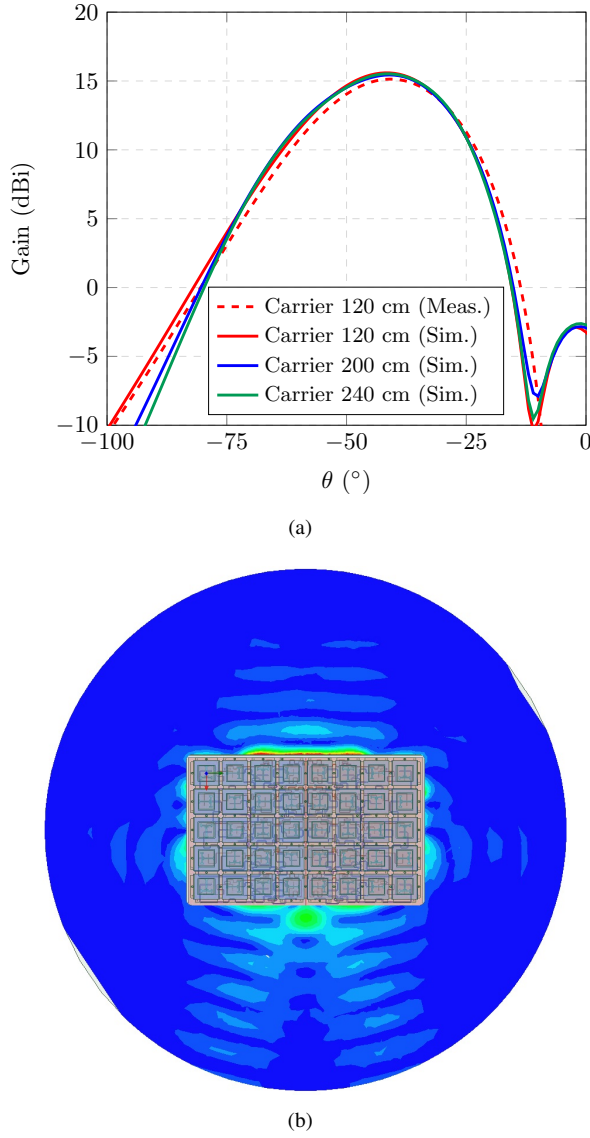
5

(a)

(b)

Figure 10: Analysis increasing the electrical size of the carrier. Horizontal polarization. (a) Main beam in elevation. (b) Induced surface currents for a carrier diameter of 200 cm.

4. Electromagnetic Bandgaps (EBGs)

Taking advantage of the surface wave suppression of the Electromagnetic Bandgaps (EBGs), the interaction between the antenna and the carrier can be mitigated, thus reducing the edge diffraction effects.

EBGs are metal-dielectric structures that are periodically arranged by the repetition of the same unit-cell (UC). In order to achieve an electrical homogenous structure at the frequency of operation, the periodicity should be way less than the wavelength. As a resonant structure, EBGs provide the suppression of surface-waves within a frequency band known as stop-band or bandgap. Due to its low-profile and planar implementation, it allows a higher degree of integration, thus becoming a suitable solution for airborne applications.

There are different types of UC designs, whose performance is optimized for broadband or multiband applications. However,
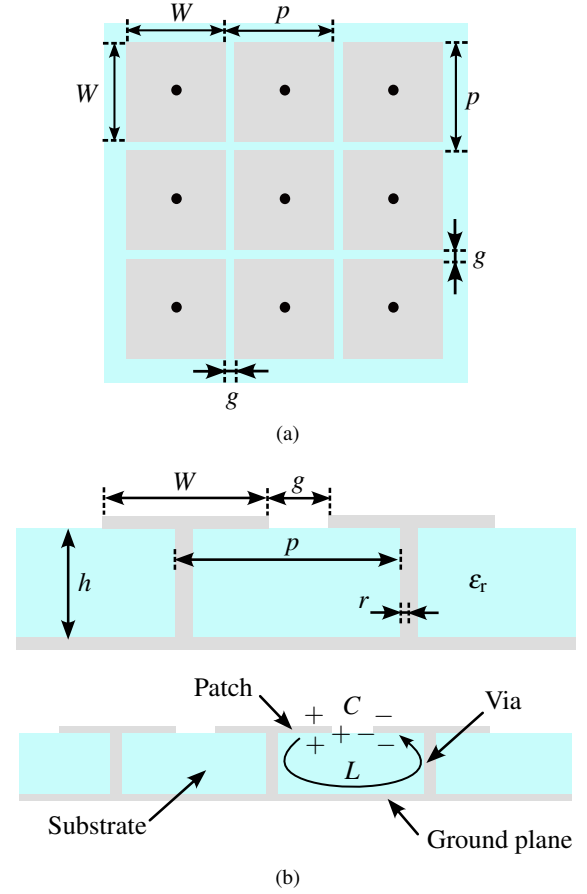

(a)

(b)

Figure 11: Geometrical arrangement of 4×4 mushroom type UC-EBG. (a) Top view. (b) Side view.

as a proof of concept, and due to its fabrication simplicity, the mushroom type UC is considered in this work.

The mushroom type UC-EBG consists of a square metallic patch of width W that is etched on a dielectric substrate of thickness h, and short-circuited to the ground by means of a via of radius r. Each unit-cell is separated to the next one by a distance g, becoming the periodicity $p = W + g$. An arrangement of 3×3 mushroom type UC-EBG is shown in Figure 11. Electrically, the overall structure, that is composed of the repetition of the same unit-cell, behaves as an LC parallel resonant circuit, in which a capacitance C is formed by the gap between patches, and an inductance L results from the current loop generated among the patches and vias. At the frequency of resonance of the equivalent LC parallel resonant circuit, i.e. $f_0 = \frac{1}{2\pi\sqrt{LC}}$, no surface wave propagates.

There are many different approaches to characterize the bandgap properties of the EBG. One of the most extended one is based on the dispersion diagram. The dispersion diagram is the graphical representation of the wavenumber, which describes the propagation of the electromagnetic waves with frequency. Due to the symmetry and the periodicity of the structure, the calculation of the wavenumbers can be limited to the so-called Brillouin zone [12].

By analyzing the dispersion diagram in the Brillouin zone, the UC can be optimized so the bandgap covers the antenna

frequency range of operation. Figure 12 shows the calculated dispersion diagram with HFSS, using the eigenmode solver and simulating one unit-cell with periodic boundaries. The geometrical parameters of the mushroom type UC-EBG, that is implemented using a substrate Isola Astra MT 77 ($\varepsilon_r = 3$, $tan\delta = 0.0017$) and thickness $h = 2.5$ mm, are listed in Table 1.

Table 1: Geometrical parameters of the manufactured mushroom type EBG.

W	39 mm	g	2.5 mm	r	2 mm	p	41.5 mm

The bandgap can be identified as the frequency range where no real wavenumber solution exists. Thus, the stopband is given by the intersection of the two first propagating modes with the light line ($|\beta| = k_0$), which approximately corresponds to 1.25-1.55 GHz.

It will be later shown that the frequency range, in which no surface wave propagates, does not entirely meet the antenna operational bandwidth. This is taken for granted, since as a resonant structure the surface wave suppression band is limited and sensitive to fabrication tolerances. Thus, in order to increase the bandgap bandwidth, thicker substrates or lower dielectric permittivites can be considered. However, due to manufacturing purposes and availability of substrate panels, the previous reported substrate material with thickness 2.5 mm has been used.
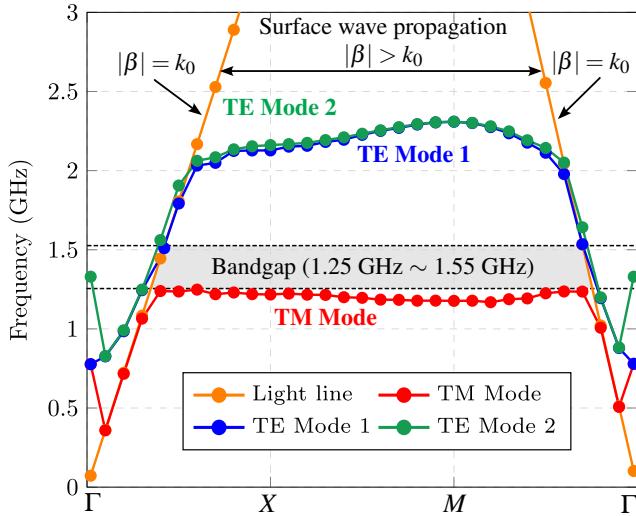

Figure 12: Calculated dispersion diagram of the proposed mushroom type UC-EBG.

5. Experimental verification of the edge diffraction effects suppression using EBGs on the antenna carrier

In order to validate the proposed approach, the optimized EBG structure has been manufactured. Despite that a conformal EBG arrangement can be also implemented [23], for testing purposes and due to manufacturing simplicity, a rectangular EBG arrangement of 6x21 unit-cells is considered in this work.

This geometrical EBG disposition is assembled by combining (for each arrangement) two EBG formations of 6x5 and one of 6x11, as depicted in Figure 13.
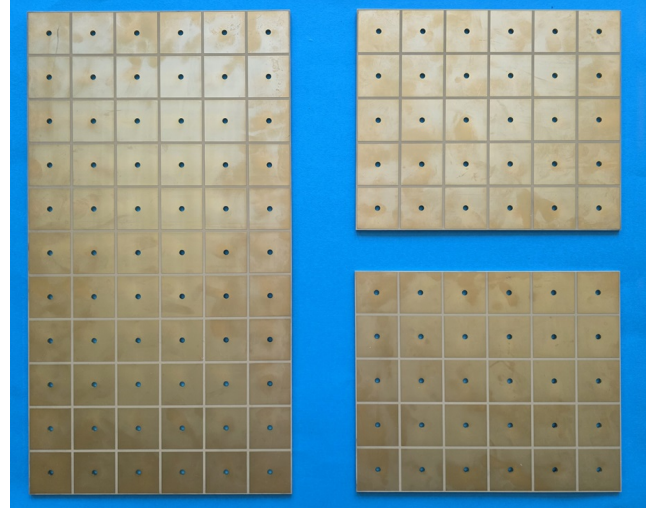

Figure 13: Manufactured geometrical arrangements of EBGs.

Due to the surface wave suppresion properties of the EBGs, the propagation of the radiated fields between antennas can be reduced, thus enhancing the isolation among them. For this reason, and besides the radiation pattern measurements, the electrical performance of the manufactured EBGs can be estimated by analyzing the coupling between two single antennas.

5.1. Analysis antenna coupling

Figure 14 shows the measurement setup using two dual-linear polarized L-band stacked patch antennas, that have been designed to test the first development stages of the final planar phased array. Both single antennas, that dispose of its own feeding to excite each polarization, are attached to a metallic plate of size 452 mm $\times$ 825 mm and thickness 2 mm. The interelement spacing is approximately 1.65λ_0, which enables enough distance to place any of the previous manufactured EBG formations among them. The same polarization definition is applied as in the case of the phased array.
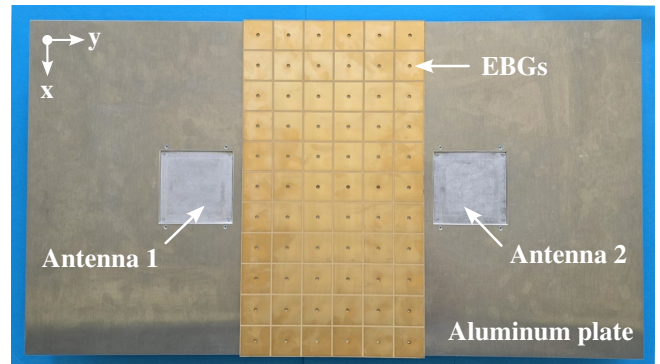

Figure 14: Measurement scenario of the coupling analysis between two dual-polarized L-band antennas.

Figure 15 shows the simulated and measured coupling levels between antennas (i.e. $|S_{21}|$), for both polarizations, with

and without the EBGs. It can be seen that for the case of the horizontal polarization, in which now an E-Plane coupling takes place, the isolation between antennas is considerably enhanced up to 15 dB in the frequency range above 1.3 GHz when using the EBGs. Be noted that the coupling levels without EBGs are already low enough, mostly below -30 dB, due to the large interelement spacing that has to be considered to assure a given number of unit-cells between antennas. It can be seen that there is a slight shift of the bandgap to higher frequencies, in comparison with the simulated results from the dispersion diagram. This slight disagreement can be explained due to fabrication tolerances. For instance, the overall substrate thickness of 2.5 mm is achieved by combining several thinner substrate layers that are bonded with adhesive foils, which may lead to some inaccuracies due to the resonant nature of the EBG. On the other side, the coupling for the vertical polarization remains comparable, due to the H-Plane coupling, as expected.

It is also worth mentioning that the coupling measurements have been performed in the CTR to avoid the inherent reflections that may occur in the laboratory, where they become more visible due to the almost omnidirectional antenna element pattern, the large wavelength, and the increased sensitivity of the low coupling measured levels.

5.2. Radiation pattern measurement with EBGs placed on each side of the antenna carrier

To suppress the surface currents induced on the antenna carrier for the vertical polarization, the manufactured EBGs are placed on the carrier surface combining the geometrical arrangements that are shown in Figure 13. Be noted that, for testing purposes, the measurements have been performed using an aluminum circular plate of diameter 120 cm and thickness 3 mm that serves as an antenna carrier replacement or mock-up. The reason for that is to avoid any possible damage of the flight-certified antenna carrier, that may occur when detaching the EBGs placed on the surface. The measured antenna with the EBGs located on the carrier surface is depicted in Figure 16.

It can be clearly seen from Figure 17 that the use of EBGs leads to a considerable suppression of the induced surface currents for the vertical polarization, and specially in comparison with the results for the carrier alone, as shown in Figure 6.

The suppression of the induced surface currents, and thus the reduction of the edge diffraction effects, is also visible in the measured radiation pattern of the vertical polarization. As it can be seen in Figure 18, the aforementioned gain reduction and main beam broadening have been not only compensated, but also slightly enhanced. Despite of the back lobe enhancement and the slight shift of the antenna main beam, probably due to the optimized performance of the EBGs at higher frequencies, it can be noted the suitability of using the considered EBGs.

The reduced interaction of the antenna with the carrier structure can be also seen in Figure 19, in which the measured total electric field in the elevation plane (XZ) for the vertical polarization is plotted. It can be noted that the intensity and propagation of the radiated electric fields, when the EBGs are located on the carrier surface, are considerably suppressed in the region $Z < 0$, proving that the interaction with the carrier edges is strongly mitigated. Be noted that the depicted lower
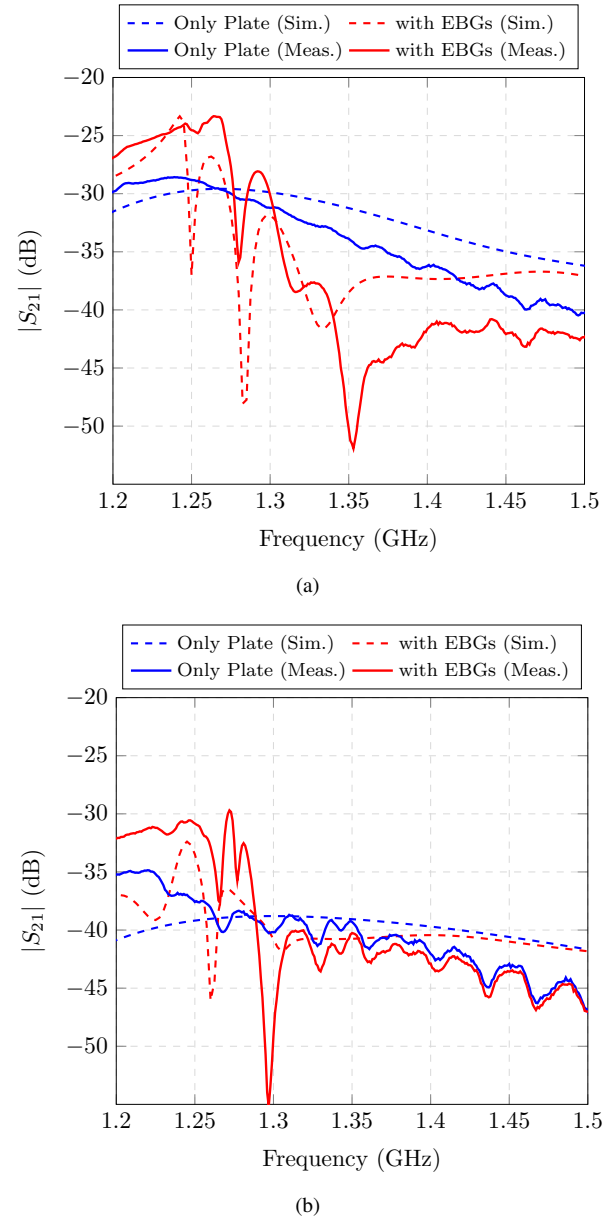

(a)

(b)

Figure 15: Analysis coupling between two dual-polarized L-band antennas (a) Horizontal polarization (E-Plane coupling). (b) Vertical polarization (H-Plane coupling).

structure of the antenna corresponds to the attachment platform required to mount the antenna onto the CTR positioner.

It is also important to mention that, due to the rectangular formation of the EBGs and the circular geometry of the carrier, the 6x5 EBG-UC arrangements of each side stick out from the carrier edge, which may affect the antenna pattern. However, the measured radiation pattern in the XZ plane with only the central EBG arrangement of 6x11 unit-cells on the carrier surface is comparable to the case considering 6x21 EBGs, as depicted in Figure 16. For this reason, it can be stated that the EBGs that stick out do not contribute to enhance the edge diffraction effects. For the sake of brevity, the comparison of both measured results is not shown.

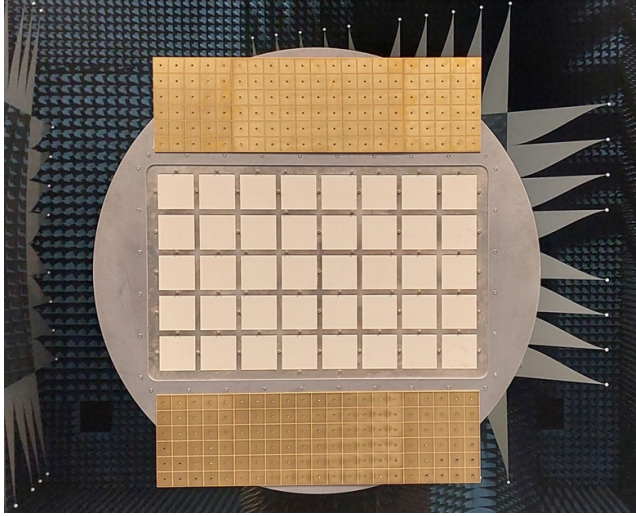On the other side, the measured radiation pattern for the

Figure 16: Measured antenna with EBGs placed on each side of the carrier surface.
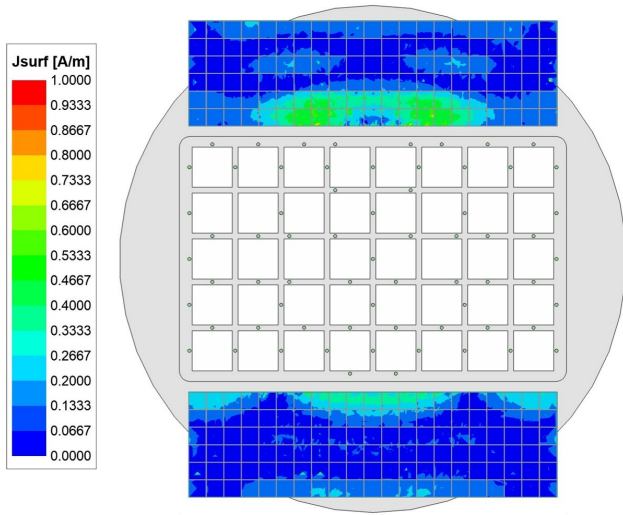

Figure 17: Reduction of the induced surface currents due to the use of EBGs. Vertical polarization. Input power 100 W.

(a)

(b)

Figure 18: Measured radiation pattern at 1.325 GHz for the vertical polarization using the EBGs on the carrier surface. Comparison with the stand-alone configuration and the carrier alone. (a) Elevation plane cut. (b) Compensation of the carrier effect using EBGs.

horizontal polarization is depicted in Figure 20. Since the position of the EBGs is mostly set to suppress the induced currents of the vertical polarization, it does not influence the radiation performance of the horizontal one, as expected. This way, similar results are achieved as if the antenna is mounted on the carrier without EBGs.

In order to provide a fairer comparison, the measured radiation pattern with the aluminum mock-up carrier is also plotted. The measured antenna gain with the thinner mock-up carrier for the vertical polarization is 0.8 dB higher than the flight-model carrier, but still slightly below than the antenna in stand-alone configuration. This can be explained due to several factors. First, the thicker carrier surface is covered with a copper mesh, which can lead to a different conductivity value than the thinner carrier, made of plane aluminum. Secondly, the flight-model carrier is a carbon-fiber reinforced polymer that could lead to some power loss if the fields propagate within the polymer
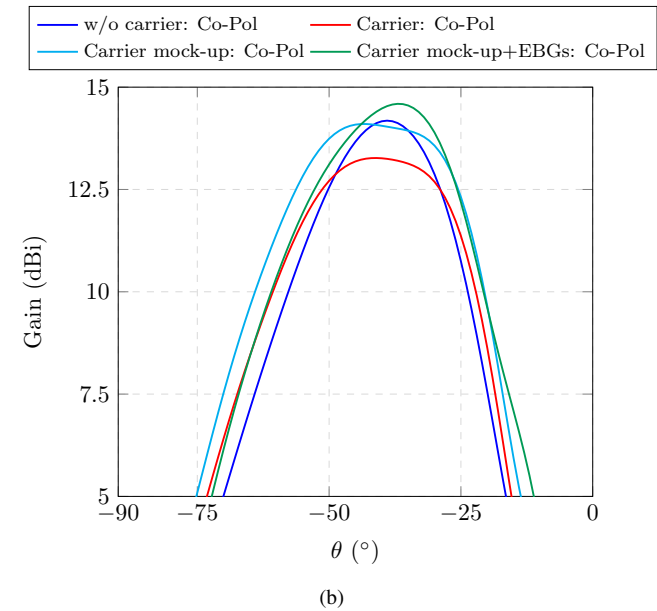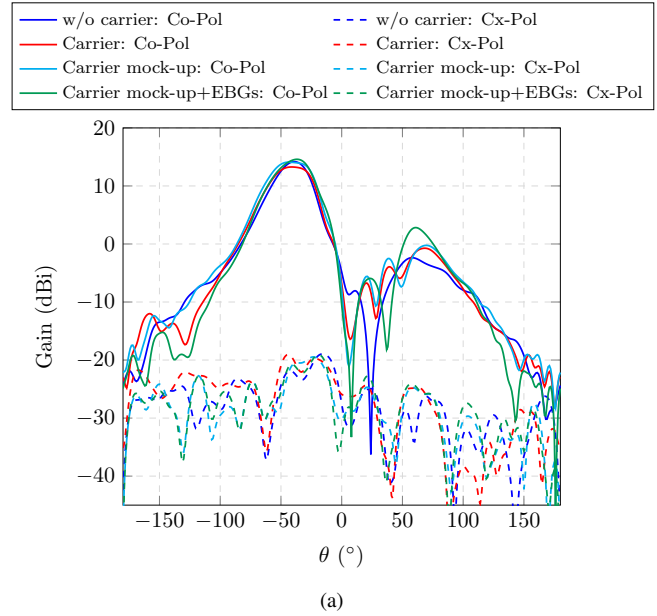
structure, since only the top side is metallized. In addition, the thinner thickness and large area of the mock-up carrier, that is only attached with screws around the antenna aperture, makes it more unstable mechanically, thus being more sensitive to misalignments and possible vibrations during measurements, which could explain the measured asymmetry in the main beam. Nevertheless, the beam widening due to the edge diffraction effects can be noted for both carriers, as well as the improvement when the EBGs are placed on the carrier surface, which validates the proposed approach.

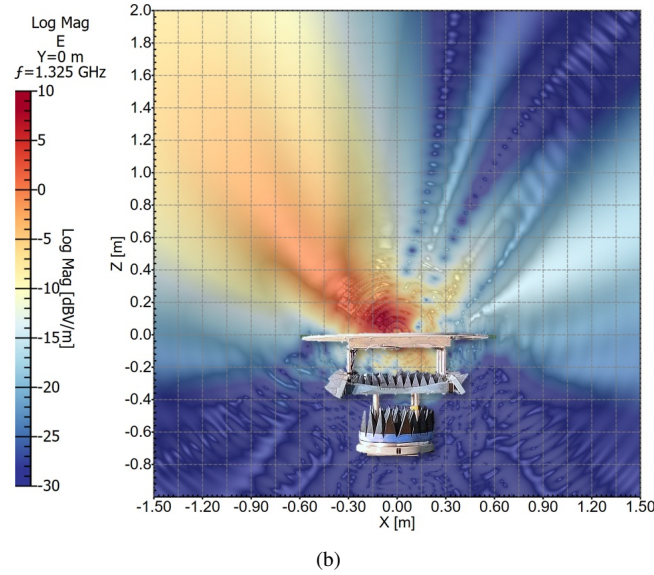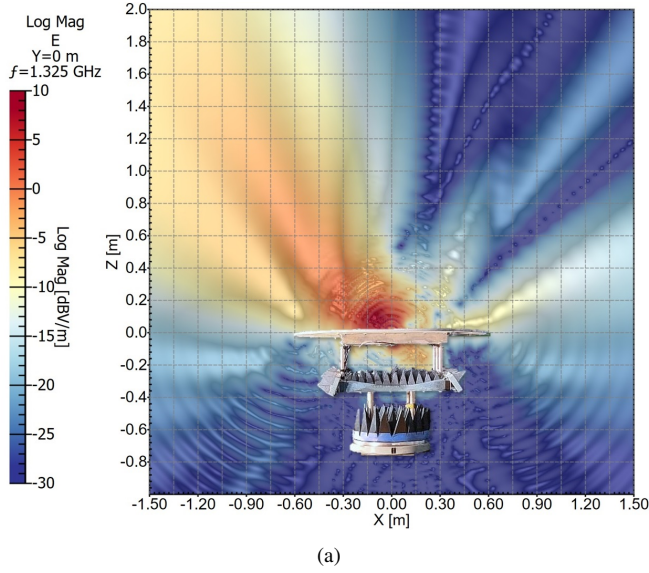Figure 21 plots the measured radiation pattern in azimuth for

(a)

(b)

Figure 19: Measured total electric field in the elevation plane. Vertical polarization. The lower antenna structure corresponds to the CTR attachment platform. (a) Carrier alone. (b) EBGs placed on each side of the carrier surface.

Figure 20: Measured radiation pattern at 1.325 GHz for the horizontal polarization using the EBGs on the carrier surface. Comparison with stand-alone configuration and carrier alone.

6. Conclusion

In this work, the polarization-dependent impact of the antenna carrier in a real airborne SAR scenario, has been presented and experimentally validated using a flight-certified phased array antenna and the carrier platform that will be installed on the aircraft. Due to the carrier geometry and the electric field direction, edge diffraction effects are more intense for the vertical polarization, leading to a noticeable main beam widening and gain reduction in the elevation plane.

In order to mitigate the antenna carrier interaction, the use of EBGs is proposed in order to suppress the surface wave propagation along the carrier, thus reducing the induced surface currents. The presented approach is validated with measurements, that make use of a rectangular geometrical arrangement of manufactured EBGs that are placed on each side of the carrier surface. This way, the edge diffraction effects for the vertical polarization are considerably reduced without interfering the performance of the horizontal case, thus compensating the aforementioned gain reduction and main beam broadening. The proposed solution allows to achieve a more balanced electrical performance for both polarizations, that is mandatory for SAR polarimetry, which also becomes independent of the antenna environment, especially relevant in airborne applications.

Further work would comprise the use of broadband EBG-UC structures to enhance the surface-wave suppression frequency range, in order to cover the antenna operational bandwidth, and becoming also more electrically robust against fabrication tolerances. In addition, a larger geometrical arrangement with more EBG-UCs could be considered that may improve, to a given extent, the presented results.

both polarizations. It can be also noted the gain enhancement when the EBGs are used for the vertical polarization, as well as a slight increase of the side lobe level. As expected, the horizontal polarization remains unaltered, except for a small increment of the cross-polarization levels, probably due to the mock-up carrier.

Thus, it can be stated that the use of EBGs allow to suppress the edge diffraction effects due to the antenna interaction with the carrier, thus achieving a more comparable radiation performance for both polarizations, that is required to apply SAR polarimetric techniques. In addition, a more independent antenna performance can be achieved regardless the antenna environment, considering not only the given carrier structure but also different geometries and larger electrical sizes.
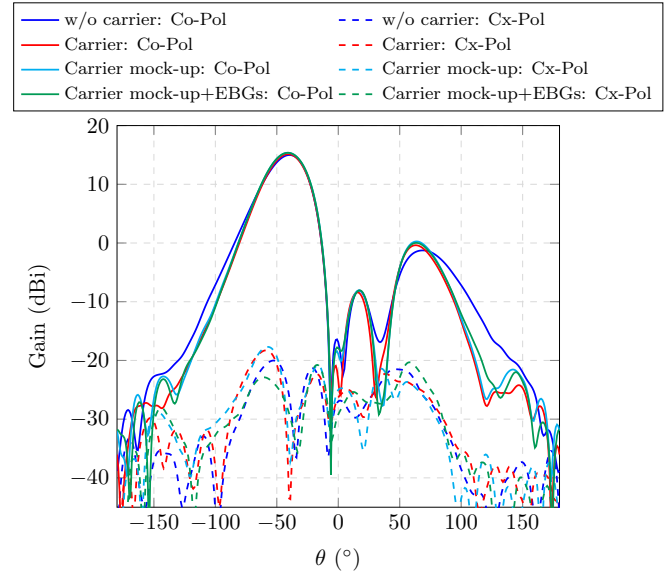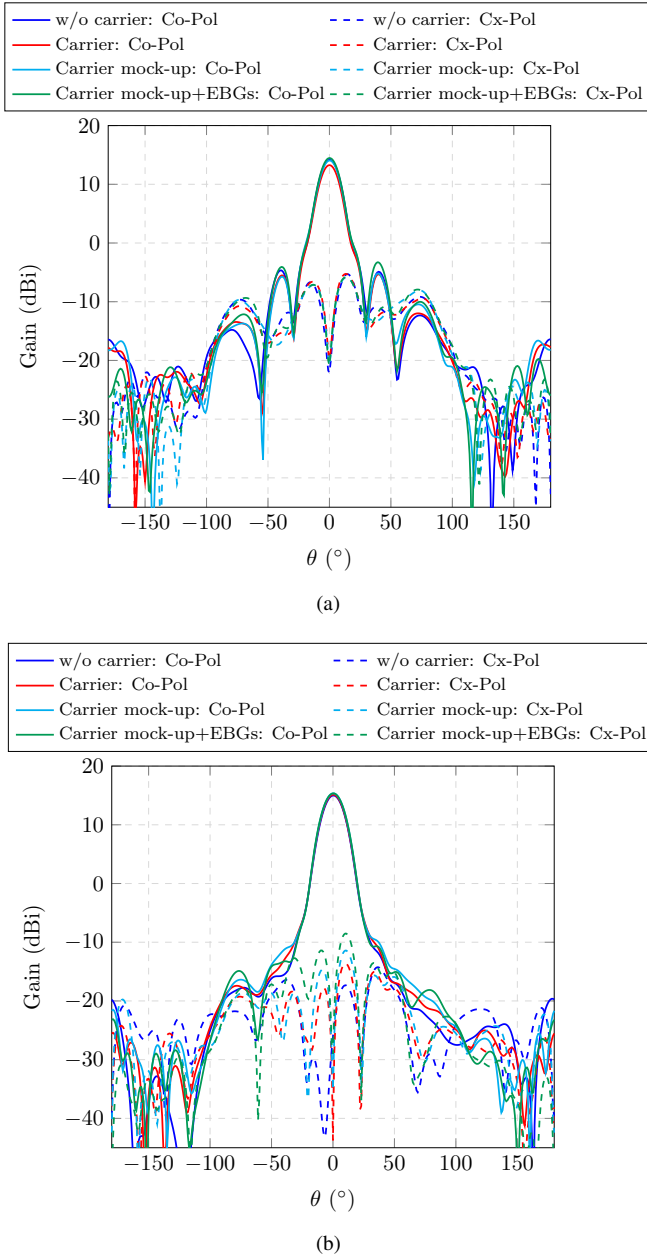
(a)

(b)

Figure 21: Measured radiation pattern at 1.325 GHz in the azimuth plane using EBGs on the carrier. Comparison with the stand-alone configuration and the carrier alone. (a) Vertical polarization. (b) Horizontal polarization.

References

[1] A. Moreira, P. Prats-Iraola, M. Younis, G. Krieger, I. Hajnsek and K. P. Papathanassiou, "A tutorial on synthetic aperture radar", *IEEE Geoscience and Remote Sensing Magazine*, vol. 1, no. 1, pp. 6-43, 2013.

[2] P. Rizzoli, M. Martone, C. Gonzalez, C. Wecklich, D. Borla Tridon, B. Bräutigam, M. Bachmann, D. Schulze, T. Fritz, M. Huber, B. Wessel, G. Krieger, M. Zink, and A. Moreira, "Generation and performance assessment of the global TanDEM-X digital elevation model", *ISPRS Journal of Photogrammetry and Remote Sensing* vol. 132, pp. 119–139, 2017.

[3] Y. Huang, Q. Zhang, and L. Ferro-Famil, "Forest height estimation using a singlepass airborne L-band polarimetric and interferometric SAR system and tomographic techniques", *Remote Sensing*, 13.3, 2021.

[4] J. Yang, Y. Yamaguchi, J. Lee, R. Touzi, and W. Boerner, "Applications of polarimetric SAR", *Journal of Sensors*, vol. 2015, 2015.

[5] A. Reigber, R. Horn, A. Nottensteiner, P. Prats, R. Scheiber, K .Bethke, and S.V. Baumgartner, "Current status of DLR's new F-SAR sensor", *8th European Conference on Synthetic Aperture Radar*, 2010.

[6] A. Reigber, E. Schreiber, K. Trappschuh, S. Pasch, G. Müller, D. Kirchner, S. Geßwein D.and Schewe, A. Nottensteiner, M. Limbach, A. Schreiber, T. Rommel, R. Horn, M. Jäger, R. Scheiber, S.V. Baumgartner, S.K. Joshi, A. Barros Cardoso da Silva, and A. Moreira, "The High-resolution digital-beamforming airborne SAR system DBFSAR", *Remote Sensing*, vol. 12, no. 11, May. 2020.

[7] Y. Zhou, W. Wang, Z. Chen, P. Wang, H. Zhang, J. Qiu, Q. Zhao, Y. Deng, Z. Zhang, W. Yu, and R. Wang, "Digital beamforming synthetic aperture radar (DBSAR): experiments and performance analysis in support of 16- channel airborne X-band SAR data", *IEEE Transactions on Geoscience and Remote Sensing*, vol. 59, no. 8, pp. 6784-6798, Aug. 2021.

[8] M. K. Emara, K. Madhoun, R. Madhoun and S. Gupta, "A low-cost light-weight 3D-printed choke ring for multipath mitigation for GNSS antennas", *2019 IEEE International Symposium on Antennas and Propagation and USNC-URSI Radio Science Meeting*, pp. 721-722, 2019.

[9] D. Lin, E. Wang, and J. Wang, "New choke ring design for eliminating multipath effects in the GNSS system", *International Journal of Antennas and Propagation*, vol. 2022, no. 1, 2022.

[10] S. Caizzone, R.A. Gerguis, E.O. Addo, S.P. Hehenberger, and W. Elmarissi, "Spatial filtering of multipath at GNSS reference stations through metamaterial-based absorbers", *IEEE Transactions on Aerospace and Electronic Systems*, vol 59.6, pp. 7764–7771, 2023.

[11] M. I. Hossain, N. Nguyen-Trong, K. H. Sayidmarie, and A. M. Abbosh, "Equivalent circuit design method for wideband nonmagnetic absorbers at low microwave frequencies", *IEEE Transactions on Antennas and Propagation*, vol. 68.12, pp. 8215–8220, 2020.

[12] D. Sievenpiper, L. Zhang, R. F. J. Broas, N. G. Alexopolous and E. Yablonovitch, "High-impedance electromagnetic surfaces with a forbidden frequency band", *IEEE Transactions on Microwave Theory and Techniques*, vol. 47, 1999.

[13] N.M. Mohamed-Hicho, E. Antonino-Daviu, M. Cabedo-Fabrés, and M. Ferrando Bataller, "A novel low-profile high-gain UHF antenna using high-impedance surfaces", *IEEE Antennas and Wireless Propagation Letters*, vol. 14, pp. 1014–1017, 2015.

[14] A.C. Durgun, C.A. Balanis, C.R. Birtcher, H. Huang, and H. Yu, "High-impedance surfaces with periodically perforated ground planes", *IEEE Transactions on Antennas and Propagation*, vol. 62.9, pp. 4510–4517, 2014.

[15] A.K. Oladeinde, E. Aryafar, and B. Pejcinovic, "MmWave Tx-Rx self-interference suppression through a high impedance surface stacked EBG", *Electronics*, vol. 13.15, 2024.

[16] N.A. Aboserwal, C. Balanis, and C.R. Birtcher, "Impact of finite ground plane edge diffractions on radiation patterns of aperture antennas", *Progress In Electromagnetics Research B* vol.55, pp. 1-21, 2013.

[17] K. A. Amusa and S. A. Adekola, "Significance of the ground plane width and frequency on the patterns radiated by rectangular slot antennas", *2021 International Conference on Electromagnetics in Advanced Applications (ICEAA)*, pp. 142-146, 2021.

[18] J. L. Salazar, N. Aboserwal, J. D. Díaz, J. A. Ortiz and C. Fulton, "Edge diffractions impact on the cross polarization performance of active phased array antennas", *IEEE International Symposium on Phased Array Systemsand Technology (PAST)*, pp. 1-5, 2016.

[19] S. Srivastava, S. M. S and A. R. Harish, "Mitigating radiation pattern ripples due to edge diffraction in central element of a large array using top hat loaded high impedance surface", *2024 IEEE International Symposiumon Antennas and Propagation*, pp. 2649-2650, 2024.

[20] J. A. Ortiz, N. Aboserwal and J. L. Salazar, "A new analytical model based on diffraction theory for predicting cross-polar patterns of antenna elements in a finite phased array", *2019 IEEE International Symposium on Phased Array System & Technology (PAST)*, pp. 1-4, 2019.

[21] T. Lan, Q. Li, Y. Dou, and X. Jiang, "A study of a wide-angle scanning phased array based on a high-impedance surface ground plane", *International Journal of Antennas and Propagation*, vol. 2019, 2019.

[22] J.A. Ortiz, "Impact of edge diffraction in dual-polarized phased array antennas", Ph.D. thesis, School of Electrical and Computer Engineering, University of Oklahoma, EEUU, 2020. [Online]. Available:https://shareok.org/handle/11244/325369.

[23] D. Lorente, M. Limbach, B. Gabler, H. Esteban and V. E. Boria Esbert, "Mitigation of the antenna carrier impact in dual-polarized phased arrays with electromagnetic bandgaps for airborne SAR sensors", *2025 19th European Conference on Antennas and Propagation (EuCAP)*, pp. 1-5, 2025.

[24] D. Lorente, M. Limbach, B. Gabler, H. Esteban and V. E. Boria, "Highly integrated low-profile multilayer dual-polarized phased array antenna with truncated cavities for first pulsed bistatic L-band airborne SAR sensor", *IEEE Access*, vol. 12, pp. 435-449, 2024.